AIP | Journal of Applied Physics

# Infrared photocurrent with one- and two-photon absorptions in a double-barrier quantum well system

Marcos H. Degani, Marcelo Z. Maialle, Paulo F. Farinas, and Nelson Studart

Citation: J. Appl. Phys. **110**, 104313 (2011); doi: 10.1063/1.3662867
View online: http://dx.doi.org/10.1063/1.3662867
View Table of Contents: http://jap.aip.org/resource/1/JAPIAU/v110/i10
Published by the American Institute of Physics.

# Infrared photocurrent with one- and two-photon absorptions in a double-barrier quantum well system

Marcos H. Degani[1,a)] Marcelo Z. Maialle,[1] Paulo F. Farinas,[2] and Nelson Studart[2]
[1]*Faculdade de Ciências Aplicadas, Universidade Estadual de Campinas - UNICAMP, R. Pedro Zaccaria, 1300, 13484-350 Limeira, SP, Brazil*
[2]*Departamento de Física, Universidade Federal de São Carlos, 13565-905 São Carlos, SP, Brazil*

(Received 7 July 2011; accepted 18 October 2011; published online 29 November 2011)

We present a theoretical investigation of a double-barrier quantum-well infrared photodetector (QWIP) having two-color selectivity. The quantum well is placed between a pair of potential barriers in order to increase selectivity through modulation of the continuum states. This also leads to a potential decrease in the dark current. Calculations are carried in the effective-mass approximation using a single-electron hamiltonian. The approach used to obtain the photocurrent yields the observation of single as well as many-photon transitions in a unified manner, by naturally accounting for real and virtual processes through intermediate states that take part in the generation of photocurrent. The two-color selectivity of the calculated photocurrent spectra comes from both one- and two-photon transitions. The performance of the system studied is compared to the results for the isolated quantum well and the advantages of the double barrier are pointed out. © *2011 American Institute of Physics*. [doi:10.1063/1.3662867]

## I. INTRODUCTION

Infrared photodetectors based on intersubband transitions in semiconductor quantum wells (QWs) have been studied for many years.[1] Quantum-well infrared photodetectors (QWIPs) are interesting systems due to the possibility of tuning the QW energy levels (subbands) simply by growth design or additionally by applying external biases. In what regards both the selectivity and sensitivity of QWIPs, it is well established that bound-to-bound transitions lead to narrower and stronger peaks in the photocurrent spectrum. In these transitions, absorption of multiple photons may be required in order for a bound electron to be transferred to the continuum of extended states. Two-photon (TP) absorptions and the associated quadratic-power optical response have been experimentally investigated for almost two decades.[2–7] The TP transitions can be achieved in different ways through intermediate states that can be either virtual or real. In the virtual case[4,5] the absorption is simultaneous and the excitation power must by stronger in order to provide a higher density of available photons. A different way of exciting TP transitions occurs via intermediate real electronic states,[6,7] in which case the complete process of photoexcitation is made up of sequential absorptions, yielding, in principle, stronger signal at lower excitation power.[8]

Aiming at more intense photocurrent signals, it is beneficial to have a strong overlap between the bound (initial) state in the QW and the extended (final) states. As proposed by some researchers, and firstly demonstrated by Kiledjian *et al.*,[9] a pair of potential barriers placed on the two sides of the QW can be used to modulate the continuum of extended states into quasibound states. These states have larger overlaps with the bound state while they are still delocalized along the growth axis allowing for current generation.

The present paper is a proposal and a theoretical study of a two-color QWIP. The use of potential barriers sandwiching the QW and the TP transitions are combined in order to enhance the selectivity. The theoretical approach is by itself innovative for the investigation of photocurrent responses in QWIPs. The calculations have been done in the effective-mass approximation considering one electron initially occupying a bound state of the QW (namely, the ground state or the first excited state). The electron interacts with an oscillating electric field oriented along the growth axis. This field plays the role of the exciting infrared light in actual devices. By following the dynamics of the initial state in time, which is done by solving numerically the time-dependent Schrödinger equation, the photocurrent spectra have been calculated. This approach naturally accounts for one- or many-photon transitions either through virtual or real intermediate states. Additional information on the energy level structure determining the photocurrent response has been obtained by the computation of the optical absorption spectra, the transmission coefficients through the QWIP potential profile and the eigenstates of the system.

The paper is organized as follows. In Sec. II, the systems investigated are presented and the theoretical method is developed. Section III presents the photocurrent spectra having contributions from one- and two-photon absorption processes under the influence of an applied bias. Section IV concludes with our discussion and final remarks.

## II. QWIP SYSTEMS AND THEORY

We have investigated QWIP systems comprising QWs sandwiched between a pair of symmetric potential barriers. For comparison, results for a QW system in the absence of barriers are also presented.

Figure 1(a) shows the potential profile of the proposed QWIP. Some of the parameters can be varied: the QW width

a)Electronic mail: marcos.degani@fca.unicamp.br.

 

($L$), the barriers' thickness ($B$), and the spacer between the barrier and the QW walls ($D$). Also, the heights of the potential offsets must be given. In the following, we consider the systems to be grown from GaAs/$GaAl_xAs_{1-x}$ semiconductor layers. Therefore, the potential heights can be given in terms of the aluminum concentration x by the empirical formula:[10]

$$V(\mathrm{x}) = 0.6(1155\mathrm{x} + 370\mathrm{x}^2)\,\mathrm{meV}. \quad (1)$$

For these materials, the electron effective mass is taken to be that of GaAs, $m = 0.067m_0$, where $m_0$ is the free electron mass, and the dielectric constant $\epsilon = 12.5$.

### A. Bound and quasibound states in the QWIP

We start by investigating a basic system of GaAs QW sandwiched between barriers of $GaAl_{0.2}As_{0.8}$. A pair of $GaAl_{0.4}As_{0.6}$ barriers, with thickness $B = 5$ nm, is used to create the quasibound states. The well width $L = 5$ nm is chosen in order to have only one bound state in the QW.

The assessment of the extended states in the continuum [states with positive energy in Fig. 1(a)] is possible by calculating the transmission coefficient through the QWIP potential, as shown in Fig. 1(b). In gray color, the transmission for the QWIP without the barriers shows a continuum of states whose density is modulated by the presence of the QW. In dark-blue color, the role of the lateral barriers is evident: they give rise to two sharp peaks (called here "quasibound states") besides modulating the continuum above the barrier. These transmission peaks are used to calibrate the energy transitions which would contribute most to the photocurrent spectra. For instance, by changing the distance $D$ between the lateral barriers and the well the energy positions of the quasibound states can be shifted.

It is interesting to observe that the QWIP with Al concentration $\mathrm{x} = 0.2$ in the underlying QW structure, and additional barriers with $\mathrm{x} = 0.4$, as shown in Fig. 1, has a predicted bound-to-quasibound transition at the wavelength 8.1 $\mu$m (~153 meV). Also, since the Al concentrations for the proposed systems can be considered small ($\mathrm{x} < 0.45$), the electronic inelastic tunneling, via the AlGaAs $X$-point band minimum is expected to play a minor role and is neglected in the present work. In fact, as it will be detailed below, incoherent scattering is neglected altogether and our treatment is based on the coherent dynamics of the electrons in the QWIP.

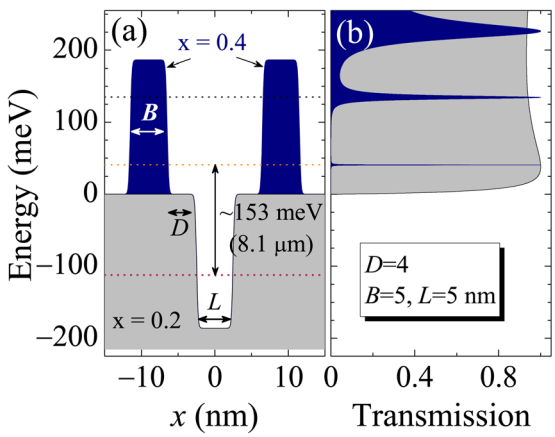


FIG. 1. (Color online) (a) Potential profiles of the QWIP with (dark blue) and without (gray) the lateral potential barriers. (b) Transmission coefficients of the structures shown in (a).

### B. Photocurrent and optical absorption spectra from the time evolution of an initially occupied state

In this section, we describe the numerical method used to obtain the photocurrent and the absorption spectra time-evolving an initially occupied state under the action of an oscillating electric field. This field, oriented along the growth axis, plays the role of the exciting infrared light in actual QWIPs. The frequency $\Omega$ of the oscillating field is related to the photon energy $\hbar\Omega$.

#### 1. Time evolution

The following one-dimensional hamiltonian is used within the effective-mass approximation for an one-electron problem in the conduction band

$$H = -\frac{\hbar^2}{2m}\frac{d^2}{dx^2} + V(x) - ex\left(F_{\mathrm{st}} + F_{\mathrm{dyn}}\sin\Omega t\right), \quad (2)$$

with the electron effective mass $m$ taken as uniform throughout the system, $V(x)$ is the potential due to the material band-offsets, $F_{\mathrm{st}}$ is a static electric field along the system axis provided by an external bias, and $F_{\mathrm{dyn}}$ is the amplitude of the applied electric field oscillating with frequency $\Omega$.

We start by calculating the ground state (or any bound state) of the system using an imaginary-time split-operator method[11] first for $F_{\mathrm{dyn}} = 0$. This solution is then taken to be the initial state $\Psi(x,0)$ to be evolved in time under the full time-dependent hamiltonian ($F_{\mathrm{dyn}} \neq 0$ in Eq. (2))

$$\Psi(x, t+\Delta t) = e^{-iH\Delta t/\hbar}\Psi(x,t). \quad (3)$$

From the many different ways to implement this operation in different orders of approximation, we have used, $e^{-i(T+V)\Delta t/\hbar} = e^{-iV\Delta t/2\hbar}e^{-iT\Delta t/\hbar}e^{-iV\Delta t/2\hbar} + O(\Delta t^3)$, where $T$ and $V$ are, respectively, the kinetic and potential operators shown in the hamiltonian given by Eq. (2). Successive applications of this operator evolves the initial wave function from $t = 0$ to a given time $t > 0$. This is the essence of the split-operator method whose details can be found in Ref. 11.

#### 2. Photocurrent spectra

Once the driving field $F_{\mathrm{dyn}}\sin(\Omega t)$ is switched on, it feeds energy into the system, and we may think of the initial $H_0$-eingenstate $\Psi(x,0)$ as evolving onto a new, dynamical, superposition of the eigenstates of $H_0$, including the continuum of extended states. This superposition depends on the frequency $\Omega$ of the excitation. There will be a greater chance of the state $\Psi(x,t)$ to be scattered out of the initially occupied state when the excitation has energy $\hbar\Omega$ matching any of the transition energies.

The time evolution of $\Psi(x,t)$ can be used to obtain the current flowing toward both sides of the system by the computation of the particle current

$$J_c(t) = \Re\left[\frac{\hbar}{im}\Psi(x,t)^* \frac{\partial \Psi(x,t)}{\partial x}\right]_{x=x_c}. \quad (4)$$

The index $c = L$ or $R$ represents current flowing toward the left or right, respectively, for which the currents are calculated at given points $x_c = x_L$ ($x_R$) in the left(right)-hand side region of the system. The current $J_c(t)$ is then integrated in time to obtain

$$I = \frac{e}{T}\int_0^T (J_R(t) - J_L(t))dt. \quad (5)$$

We refer to this current as "photocurrent," which can be presented as a function of the excitation energy ($\hbar\Omega$) in a photocurrent spectrum. Positive (negative) values of $I$ indicates an overall current flowing toward the right (left).

Our numerical method utilizes hard-wall boundary conditions, that is, the wavefunction must vanish at the boundaries of the system.[11] With the energy input given by the driving (oscillating) field, the superposition tends to become predominantly made up of higher energy, extended states and eventually the current becomes nonzero. In this case, the wavefunction reaches the boundary of the system, causing reflection and interference in the current. In order to avoid these spurious effects,[12] we have employed exponential imaginary-potential barriers[13] to absorb the energy excess near these boundary regions.

One point to be considered for the use of Eq. (5) refers to the ionization of the initial state by the action of the driving field. For instance, if we consider intense excitation (intense $F_{\mathrm{dyn}}$) or longlived excitations (long $T$), it is expected that the initial state $\Psi(x,0)$ eventually becomes ionized and absorbed by the imaginary potential barriers at the boundaries. In such a case, the current $J_c(t)$ in Eq. (4) tends to zero and the integrated current $I$ in Eq. (5) starts to decrease due to the pre-factor $1/T$. This limiting cases are avoided in our calculations by probing the system with driving field for times $T$ short enough to ensure the ionization effects do not commence. In fact, we have observed that the current $J_c(t)$ increases approximately linearly in time for initial times, i.e., before ionization effects commence. Therefore, the current $I$, calculated from Eqs. (4) and (5), becomes $T$-independent for $T$ chosen in this early stage of the excitation dynamics.

### 3. Optical absorption spectra

The time evolution of the wavefunction can also be used to calculate the optical absorption for an electron occupying initially a given bound eigenstate $\psi_n(x)$ of the QWIP with energy $E_n$. The absorption spectrum is obtained from the Fourier transform of the time-correlation of the electric dipole $d(t)$, which is computed as follows. First, an initial state $\psi_F(x,t=0)$ is calculated when a bias is applied to the system (i.e., $F_{\mathrm{st}} \neq 0$ and $F_{\mathrm{dyn}} = 0$). Then, the bias is turned off ($F_{\mathrm{st}} = 0$ and $F_{\mathrm{dyn}} = 0$) and the state is evolved in time yielding $\psi_{F=0}(x,t_+)$, with $t_+ = t > 0$. Again, the time evolution is done by the same split-operator method described before. The dipole element in question is a time-correlation of $\psi_{F=0}(x,t_+)$ with any given eigenstate $\psi_n(x)$ representing the initially occupied bound state in the QWIP from which the absorption takes place, that is,

$$d_n(t) = \int [\psi_n(x)e^{-iE_n t/\hbar}]^*(-ex)\psi_{F=0}(x,t_+)dx. \quad (6)$$

One can see how the absorption spectra arises from Eq. (6) if the states are decomposed (this is *not* done in our numerical procedure) in terms of the eigenstates of the system. The absorption coefficient $\alpha_n(\omega)$ can then be obtained from $d_n(\omega) = \alpha_n(\omega)F(\omega)$, where

$$d_n(\omega) = \sum_p a_p \int e^{i[\omega - E_n/\hbar]t} d_p(t)dt, \quad (7)$$

and $F(\omega)$ is the Fourier transform of the applied bias $F(t) = F_{\mathrm{st}}\,\Theta(-t)$, with $\Theta(-t)$ being the Heaviside step function. The argument in the exponential of Eq. (7) $(\propto E_p - E_n)$ shows the spectral structure of $\alpha_n(\omega)$. As already noted, our numerical procedure does not make the decomposition suggested in Eq. (7). Instead, only the bound state $\psi_n(x)$ and the time evolved state $\psi_{F=0}(x,t_+)$ need to be computed and used in Eq. (6), and then, $\alpha_n(\omega)$ is obtained from a fast-Fourier transform on $d_n(t)$.

## III. RESULTS AND DISCUSSION

In Fig. 2(a) we find the photocurrent spectra for the system shown before in Fig. 1(a). The initial state $\Psi(x,0)$ is taken as the ground state of the QWIP, which is a state bound to the QW. The energy axis corresponds to the frequency of the oscillating field, i.e., $\hbar\Omega$, and the graphs were obtained for $T = 1$ ps and $F_{\mathrm{dyn}} = 5$ kV/cm. As discussed before, for

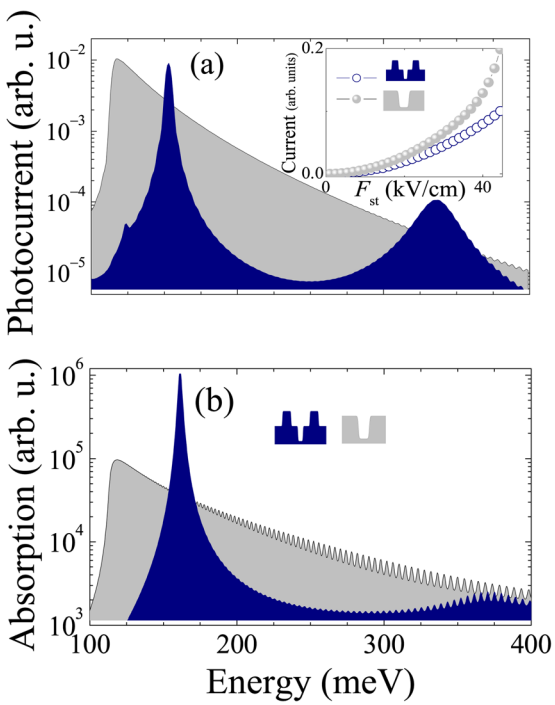


FIG. 2. (Color online) (a) Photocurrent spectra and (b) the absorption spectra for the QWIPs shown in Fig. 1(a). Both spectra are shown in logarithm scale. In all graphs, the initial state used in the calculations is the ground state. Inset: Leaking current as function of the applied bias $F_{\mathrm{st}}$.

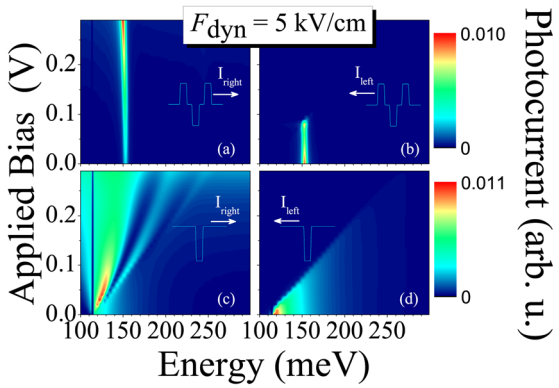


FIG. 3. (Color online) Photocurrent spectra for different applied bias $F_{st}$ and oscillating field intensity $F_{dyn} = 5$ kV/cm, for the QWIP (a,b) with and (c,d) without the lateral barriers. (a,c) Current flowing toward the right. (b,d) Current flowing toward the left.

these values of $T$ and $F_{dyn,}$ the current $J_c(t)$ does not show ionization effects and the photocurrent $I$ is $T$-independent. The increase of $F_{dyn}$ will be discussed below with Fig. 4.

Comparison of the photocurrent spectra in Fig. 2(a) for the QWIP with (dark blue) and without (gray) the pair of potential barriers demonstrates that the barriers concentrate the current signal around two excitation frequencies, with the peak at $\hbar\Omega \sim 153$ meV having $I$ about 100 times stronger than the peak at ~340 meV. The peak at ~153 meV is due to the transition from the ground state to the lowest-energy quasibound state [cf. Fig. 1(a)]. A similar transition reaching the second lowest-energy quasibond state is prohibited by the selection rule involving the parities of the wavefunctions. This comes out naturally from the numerical procedure of evolving the wavefunction in time, as it was described above. The peak at ~340 meV is due to the direct transition reaching the continuum above the lateral potential barriers. Therefore, as expected, the lateral barriers increase the frequency selectivity.

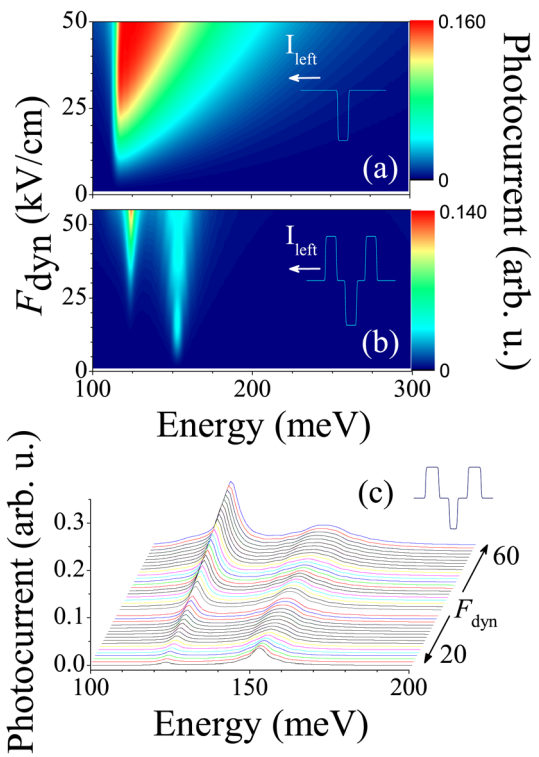


FIG. 4. (Color online) Photocurrent spectra for zero applied bias ($F_{st} = 0$) and different intensities of the oscillating field ($F_{dyn}$), for the QWIPs (a) without and (b) with the lateral barriers. (c) The same as in (b) but in waterfall format.

Potentially, the barriers also reduce the dark current in actual QWIP devices because the frequency selectivity inhibits phonon absorption. To give a qualitative estimate of how this spectral limitation would contribute to reduce the dark current, the current leaking the QWIP was calculated for no excitation ($F_{dyn} = 0$) but under nonzero applied bias $F_{st.}$ This is shown in the inset of Fig. 2(a), for the systems with and without the lateral barriers, from where it is noted that the barriers indeed reduced the leak of current under applied bias. This statement, based solely on the calculated leaked current, is of course sketchy because the dark current in actual QWIP can have many other contributions (such as phonon scattering) not considered in the calculations resulting in the inset of Fig. 2(a).

The absorption spectra shown in Fig. 2(b) are very similar to the photocurrent spectra in Fig. 2(a). For both types of spectra, due to the quasibound states created by the lateral barriers, there is a selected range of frequencies contributing most to the spectra. A closer look at Fig. 2 reveals a spectral shift between the photocurrent and the absorption spectra, for the system with barriers, specially with respect to the second peak (~350 meV). This shift results from the different approaches used to obtain both spectra. In the case of the absorption spectra, Fig. 2(b), the wavefunction $\Psi(x,t)$ is evolved in time without any applied field. On the other hand, the photocurrent spectra, Fig. 2(a), are calculated under the action of the driving oscillatory field $F_{dyn,}$ which can lead to spectral shift: the so-called "dynamical Stark shift."

The photocurrent spectra shown in Fig. 2(a) are in fact half of the sum of the absolute values of the two currents flowing toward both sides of the QWIP structure. These two contributions are the same (not considering the sign) since the potential is symmetric in space, yielding no effective current, i.e., $I = 0$ from Eq. (5). A bias (an external electric field) is usually applied to the QWIP in order to direct the photocurrent to one specific direction, therefore, yielding a nonvanishing effective current. Bias is also used to externally control the QWIP energy levels and consequently shifting the resonant frequencies.

We have investigated the effects of a static electric field applied along the system axis. For that, a positive bias (i.e., field favoring current directed toward the right) was applied to the QWIP. Figure 3 shows the photocurrent flowing toward the right [Fig. 3(a)] and toward the left [Fig. 3(b)] for the QWIP with barriers. It is observed that the stronger photocurrent peak at ~150 meV remained spectrally pinned under the application of the bias. On the contrary, the QWIP without the lateral barriers, as seen from Figs. 3(c) and 3(d), showed a broader photocurrent spectra very dependent upon the applied bias.

The effects of the intensity of the driving field $F_{dyn}$ are shown in Fig. 4. The spectra for the QWIP without the barriers, Fig. 4(a), show that increasing $F_{dyn}$ basically causes

an enhancement and a further broadening of the photocurrent peak. An entirely different behavior is seen for the QWIP with barriers. In Fig. 4(b), the increase of $F_{dyn}$ also broadens the photocurrent peak at ~150 meV, but most interestingly, a new peak appears for high excitation intensities $F_{dyn} > 25$ kV/cm at the energy ~125 meV (actually at 123.4 meV or wavelength of 10.1 $\mu$m). This peak was already present in the (log-scale) spectra of Fig. 2(a) as a small peak (since there $F_{dyn} = 5$ kV/cm) on the lower-energy shoulder of the 150-meV peak. The intensity of the 125-meV peak increases rapidly with the increase of $F_{dyn}$, as it is clearly seen from Fig. 4(c). It is interesting to note that an excitation with energy ~125 meV will promote an electron from the ground state of the QW to the continuum where the transmission coefficient is very small (cf. Fig. 1), therefore, tunneling (and current) is expected to be equally unlikely in this energy range. The question that arises is then about which process is responsible for the 125-meV peak.

One clue to find the answer is the fact that twice the peak energy, i.e., ~250 meV, is the transition energy between the ground state and the *second* quasibound state (cf. Fig. 1. This was the forbidden transition mentioned before). Therefore, a TP absorption at ~125 meV can excite the electron to the second quasibound state. To check this hypothesis, we have plotted in Fig. 5(a) the heights of the peaks in the photocurrent spectra as functions of the amplitude $F_{dyn}$ of the driving field. For the QWIP without the lateral barriers [gray-colored symbols in Fig. 5(a)], the only existing peak of the photocurrent spectra grows as $F_{dyn}^2$, which is consistent with a linear absorption process that scales with the excitation power ($\sim F_{dyn}^2$). We can associate this excitation with an one-photon process generating photocurrent. For higher values of driving fields, $F_{dyn} > 20$ kV/cm, the photocurrent saturates, as already explained, due to the complete ionization of the initial state. The decrease of the signal at even higher $F_{dyn}$ is related to Rabi oscillations resulting from the coherent excitation dynamics captured by our method. For the QWIP with barriers, Fig. 5(a) shows the growth of the two peaks, at ~125 meV and ~150 meV [blue and white symbols in Fig. 5(a), respectively]. The 150-meV peak increases similarly to the one in the QWIP without barriers, i.e., $\sim F_{dyn}^2$. This is again associated with an one-photon transition. Now the 125-meV peak grows as $\sim F_{dyn}^{3.5}$, that is, almost quadratic with the excitation power. This growth is consistent with nonlinear processes in which two photons are absorbed. The power dependency is not exactly $F_{dyn}^4$ because the excitation at ~125 meV can couple the initial state directly with the continuum, although via states having very small tunneling probabilities, as already seen from the study of the transmission coefficients.

The picture that emerges for the transitions in the QWIP with barriers is that shown in Fig. 5(b). The photocurrent is more intensively created by transitions reaching the first quasibound state (one-photon transitions) or the second quasibound state (TP transitions). The proposed QWIP with barriers, under high intensity light, can function as a two-color infrared detector, for both wavelengths: 8.1 $\mu$m (one-photon) and 10.1 $\mu$m (TP).

The TP transition at 10.1 $\mu$m discussed so far was mediated by the occupation of virtual states. If these states were

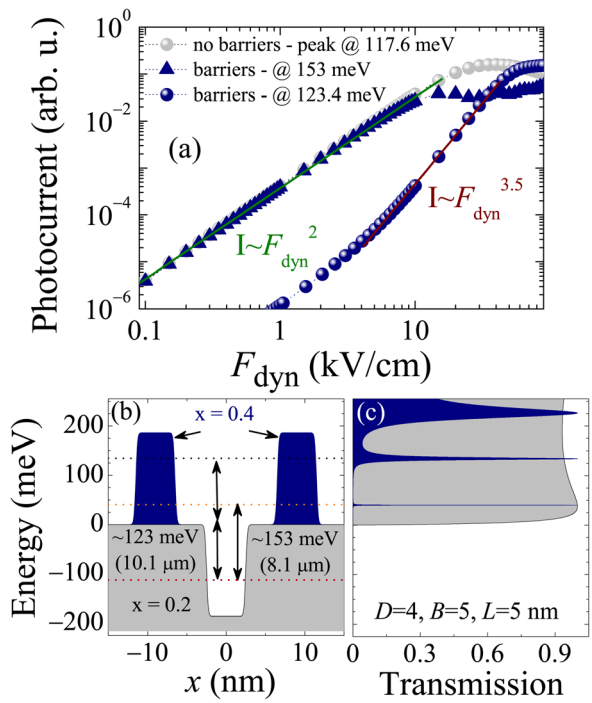


FIG. 5. (Color online) (a) Intensities of the photocurrent peaks associated with the one-photon and two-photon transitions. (b) Potential profile of the QWIP investigated [the same as in Fig. 2(a)] with the schematics indicating the one-photon and two-photon transitions. (c) Transmission coefficient.

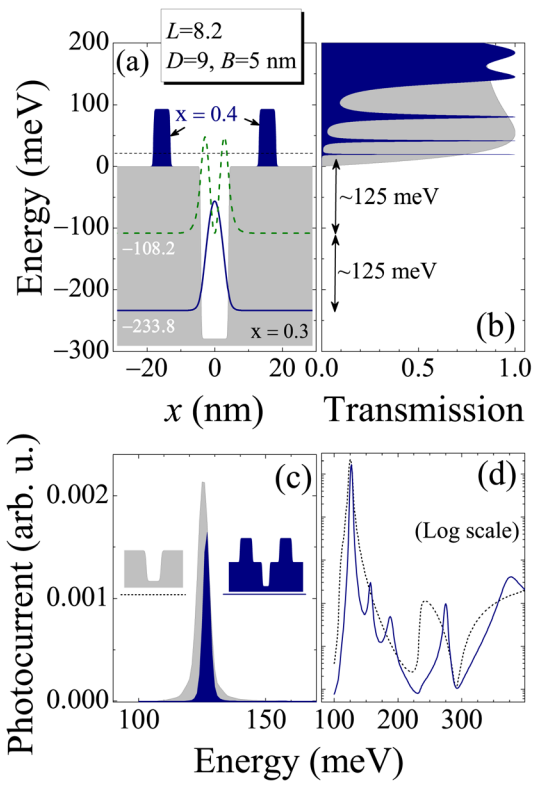


FIG. 6. (Color online) (a) Potential profile and (b) transmission coefficient of the QWIP system which allows for two-photon sequential transitions at ~125 meV (~10.1 $\mu$m). (c) Photocurrent spectrum calculated for the QWIP system in (a). (d) Same as in (c) but in logarithm scale. The driving field amplitude used is $F_{dyn} = 5$ kV/cm.

real ones, the TP process could be seen as sequential absorptions of photons, with the state $\Psi(x,t)$ occupying an existing intermediate state during excitation. A stronger current signal is expected from TP processes mediated only by real states than for the case involving virtual states.[8]

In order to explore this possibility, the system was redesigned to accommodate two bound states in the QW, but in such a way that the three lowest-energy states were energetically equidistant from each other. Figure 6(a) shows one possible QWIP with this characteristic. The system's dimensions and material composition are: $L = 8.2$ nm, $D = 9$ nm, $B = 5$ nm, $x_{barrier} = 0.4$, and $x = 0.3$, as it is also shown in Fig. 6(a). The corresponding transmission coefficient is shown in Fig. 6(b) for the QWIP with and without the lateral barriers. As it can be seen, the first excited bound state is $\sim 125$ meV above the ground state and $\sim 125$ meV below the first quasibound state created by the barriers.

The calculated photocurrent spectrum for the QWIP in Fig. 6(a), having the initial state as the ground state, is shown in Fig. 6(c). The spectrum clearly shows that the TP transition at $\sim 125$ meV is dominant. For comparison, note that the lowest-energy one-photon transition is expected at $\sim 275$ meV, which is the transition from the ground state to the second quasibound state (transition to the first quasibound state is prohibited by the parity selection rule). In Fig. 6(c), at $\sim 275$ meV, there is indeed a small photocurrent peak, but much smaller than the one at $\sim 125$ meV. The fact that the TP process produces stronger photocurrent signal than the one-photon transition, even at relatively low excitation power (here, $F_{dyn} = 5$ kV/cm), has been reported in the literature for quite some time.[7] The whole photocurrent spectrum can be better visualized in the logarithm scale of Fig. 6(d). For the system with barriers (blue line), there are three peaks for energies below 200 meV which are related to TP transitions accessing the three lowest-energy quasibound states [cf. Fig. 6(b)]. In this case, note that the lowest-energy peak is much stronger than the other two peaks since it results from a TP transition involving an intermediate real state, whereas the others involve virtual states. The peak at $\sim 275$ meV is related to the one-photon process discussed above, and the broader peak above 300 meV results from one-photon transition directly to the continuum and above the lateral barriers.

The photocurrent signal due to TP absorption for the system in Fig. 6(a) can be improved by moving the quasibound state to higher energies, where the states tunnel easily to the continuum. Wishing to keep the TP peak at $\sim 125$ meV ($\sim 10.1$ $\mu$m), a new system is proposed with parameters: $L = 7$ nm, $D = 3.2$ nm, $B = 5$ nm, $x_{barrier} = 0.4$, and $x = 0.2$, as it it shown in Fig. 11(a). The transmission coefficient in Fig. 7(b) shows only one quasibound state at higher energy. The photocurrent spectrum around the TP transition for this

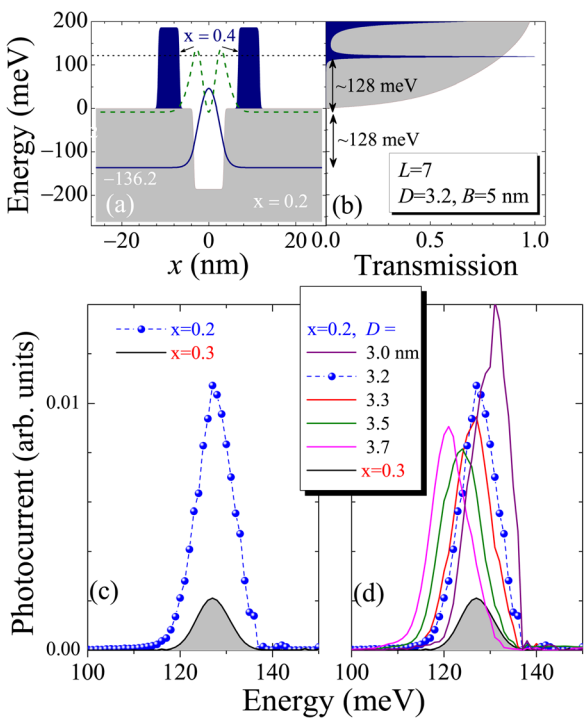


FIG. 7. (Color online) (a) Potential profile and (b) transmission coefficient of a different QWIP system with the quasibound state at higher energy. The level structure allows for two-photon sequential transitions at $\sim 125$ meV ($\sim 10.1$ $\mu$m). (c) Photocurrent spectra around $\sim 125$ meV calculated for the QWIP system in (a) (blue symbols) and for the system in Fig. 6(a) (red symbols). The driving field amplitude used is $F_{dyn} = 5$ kV/cm. (d) Photocurrent spectra around $\sim 125$ meV calculated for the QWIP system in (a) for different values of the spacer $D$ and for the system in Fig. 6(a) (solid red).

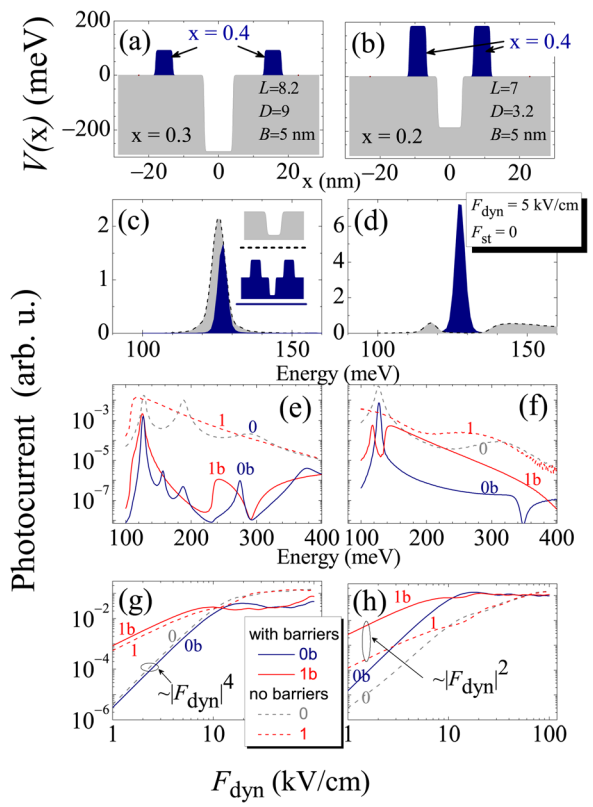


FIG. 8. (Color online)Results for the systems presented in Fig. 6 (left panels) and in Fig. 7 (right panels). (a,b) Systems' potential profile. (c,d) Photocurrent spectra showing a strong peak due to two-photon sequential absorption. In blue, are the results for the QWIP with lateral barriers and in red without the barriers. (e,f) Photocurrent spectra in logarithm scale. Solid (dashed) lines are for the initial states being the ground state (first excited state). Blue (red) colored lines are for the QWIP system with (without) the lateral barriers. (g,h) Photocurrent peak maximum value as function of the driving field amplitude.

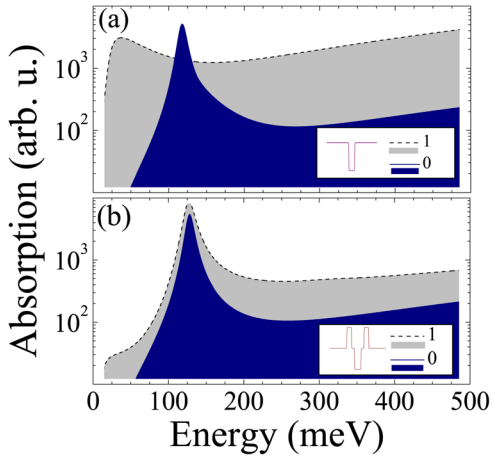


FIG. 9. (Color online) Absorption coefficient for the systems presented in Fig. 7 without (a) and with (b) the lateral barriers, for the initial state being either the ground state (blue) or the first-excited state (red).

system is shown by blue symbols in Fig. 7(c), together with the one (red symbols) previously shown in Fig. 6(c). An improvement in the current intensity is clearly observed. In Fig. 7(d) the spectra for this system are shown for slightly different values of the spacer $D$, demonstrating that further improvement is possible by adjusting the system's parameters.

A comparison between the two systems just discussed is summarized in Fig. 8. On the left panels [Figs. 8(c), 8(e), and 8(g)] are the spectra for the system previously shown in Fig. 6, and on the right panels [Figs. 8(d), 8(f), and 8(h)] are the photocurrent spectra for the system previously shown in Fig. 7. Both systems have a strong photocurrent peak at ~125 meV due to TP transitions, but the latter has an improved performance as shown before in Fig. 7(c). Figures 8(c) and 8(d) demonstrate again the better performance of the system with quasibound states at higher energies.

In Figs. 8(e) and 8(f), the (log-scale) spectra were calculated with the initial state being either in the ground state (solid lines) or in the first excited state (dashed lines). Without the lateral barriers (red colored lines), the occupation of the first excited state seems to dominate the spectra and to introduce additional broadening. In an actual situation, the spectra can have contributions from both initial states, maybe with different weights for the occupations, for instance, due to thermal effects. Interestingly, the systems with lateral barriers show strong photocurrent peaks at ~125 meV *for both types of occupation*. If the initial state is the ground state, then, a TP transition leads to the peak at ~125 meV as discussed before, but if the excited state is the initial state, the peak remains at ~125 meV, however, being due to a one-photon transition. The barriers and the TP transitions, therefore, ensure the photocurrent peak to remain at ~125 meV even for excited-state initial occupation.

The absorption spectra calculated with these two types of initial occupation also demonstrate this fact. In Fig. 9(a), for the QWIP of Fig. 7 without the lateral barriers, the absorption spectra for the two initial occupations are quite different, each covering distinct regions of the spectrum. On

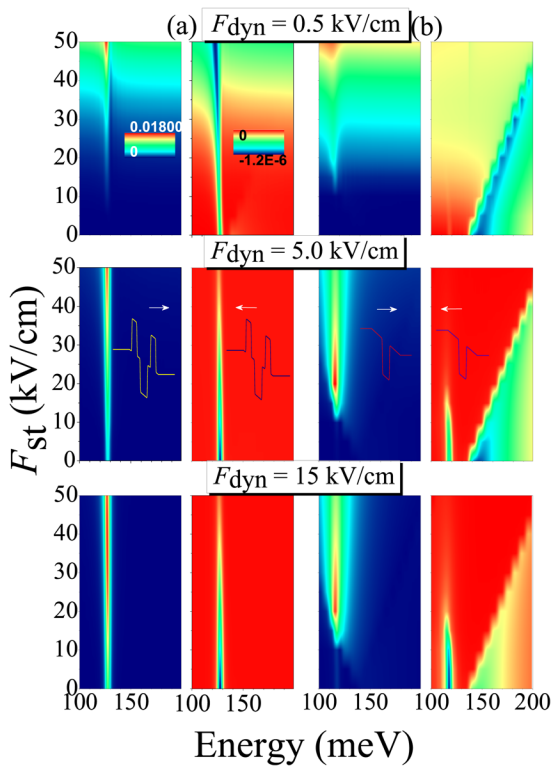


FIG. 10. (Color online) Bias dependence of the photocurrent spectra of the QWIP proposed in Fig. 7, with (a) and without (b) the lateral barriers, for different values of the driving field amplitude $F_{dyn.}$ In (a) and (b), the panels at the right (left) are for current flowing to the left (right), that is, contrary (along) the applied bias. The initially occupied state is the ground state.

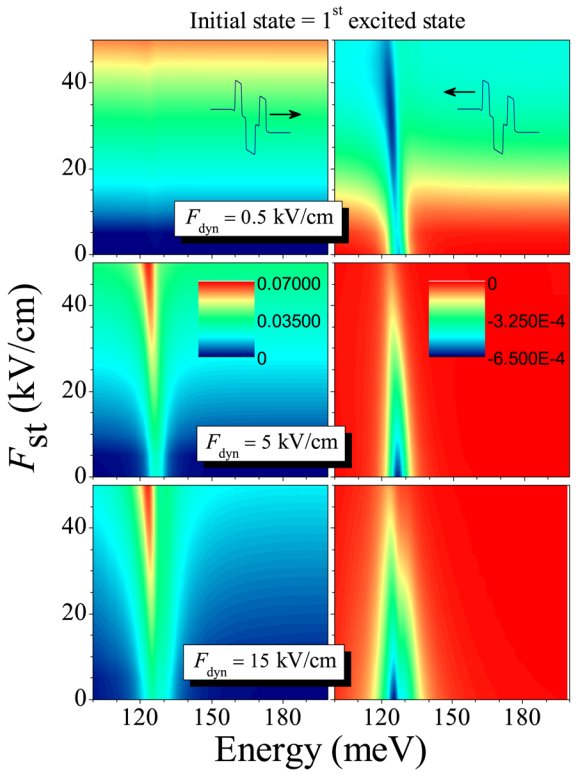


FIG. 11. (Color online) Bias dependence of the photocurrent spectra of the QWIP proposed in Fig. 7, for different values of the driving field amplitude $F_{dyn.}$ Values of the photocurrent in arbitrary units. Panels at the left (right) column are for current flowing to the left (right). The initially occupied state is the *first-excited* state.

the other hand, in Fig. 9(b), for the QWIP of Fig. 7 with the lateral barriers, the two initial occupations lead to an almost overlapping spectra, both enhancing the spectral region around ~125 meV.

Figures 8(g) and 8(h) show how the photocurrent peak maximum at ~125 meV behaves as a function of the amplitude $F_{dyn}$ of the driving field, for both types of initial state occupation. The slopes of the log-scale graphs tell us that if the initial state is the ground state, then, a TP transition gives rise to the photocurrent, whereas if the initial state is the first-excited state, then, an one-photon transition is sufficient.

The application of a bias to the QWIP of Fig. 7 is investigated in Fig. 10, for different values of the driving field $F_{dyn}$, and for the QWIP with [Fig. 10(a)] and without [Fig. 10(a)] barriers. The initial occupation in Fig. 10 is the ground state. Similar results for the QWIP with barriers, but with the initial state being the first excited state is shown in Fig. 11. What can be extracted from these figures is the virtual absence of spectral shifts for the peak near ~125 meV in a wide range of applied biases.

## IV. CONCLUSIONS

In conclusion, a QWIP system [Fig. 1(a)] has been proposed to function as a two-color infrared detector. The proposed system benefits from the high sensitivity given by the use of lateral potential barriers and, additionally, by the excitation of TP transitions. The two strongest peaks in the photocurrent spectra (Fig. 4) can be adjusted to work in the wavelength of ~10.1 $\mu$m (TP transition) and ~8.1 $\mu$m (one-photon transition). The numerical method used to investigate the photocurrent spectra is an original approach which allowed us to obtain the photocurrent signal for the one- and TP absorptions in a unified manner. Recently, the same method was successfully applied to a three-dimensional system, namely, a quantum-dot infrared photodetector (QDIP).[8] Additional information has been obtained from the optical absorption spectra, from the transmission coefficients and from the energy level structures of the QWIPs investigated. All the above, with the exception of the transmission coefficients, derived from the same numerical procedure, namely, the split-operator method.[11] Another QWIP [Fig. 7(a)] with very high sensitivity was proposed to work at ~10.1 $\mu$m, which is based on the absorption of two photons. In this case, the photocurrent intensity can be improved by allowing the existing (real) states to serve as intermediate steps in the TP process. Additionally, we have studied the signal originating from the occupation of the first-excited state and found that these contributions should lead to the same overall results since the photocurrent generated is within the same spectral region excited by the TP transitions coming from ground state occupations. The systems proposed have been investigated under the action of an external bias and the important features observed in the photocurrent spectra seem to remain dominant for a wide range of applied bias. We have not included finite temperature or carrier-density effects that will take place in actual QWIP devices due to, e.g., electron-phonon and electron-electron scatterings. Scattering events may modify the excitation dynamics of the energy-level *occupation*, however, they are not expected to substantially modify the energy-level *structure*, which has been revealed in our photocurrent calculations. Since our study is focused on the theoretical investigation of the physical processes involved in possible (proposed) QWIP structures, various practical issues related to the actual detector are beyond the scope of the present work. It is worth nonetheless noticing (Figs. 4 and 5) that the two-color peaks are very narrow and, especially, the multi-photon processes involved in their generation lead to a quite strong difference in the power-law dependence these peaks follow with the applied bias (Figs. 5(a) and 4(c)). This means that the spectral cross-talk in an actual device is expected to be controllable with an external bias. Due to the significant difference in the power-law behavior attached to the different absorption processes leading to the two peaks, we expect it to be possible to keep a device working in regimes of low cross-talk by simply turning the bias from zero to a preset value in the higher-field end of the spectra shown in Fig. 4(c) in order to switch between the two-color channels, while for intermediate values of the field, the spectral cross-talk is expected to be higher.

## ACKNOWLEDGMENTS

The authors are grateful to D. William, A. A. Quivy, E. C. F. da Silva, M. P. Pires, P. L. de Souza, J. M. Villas-Boas, and P. S. S. Guimarães for useful discussions. This work was supported by DISSE—Instituto Nacional de Ciência e Tecnologia de Nanodispositivos Semicondutores and CNPq—Conselho Nacional de Desenvolvimento Científico e Tecnológico, Brazil. M.H.D. and M.Z.M. wish to thank FAPESP for financial support.

[1] B. F. Levine, J. Appl. Phys. **74**, (8) R1 (1993).
[2] J. Khurgin and S. Li, Appl. Phys. Lett. **62**, 126 (1993).
[3] S. Li and J. Khurgin, J. Appl. Phys. **73**, 4367 (1993).
[4] H. C. Liu, E. Dupont, and M. Ershov, J. Nonlinear Opt. Phys. Mater. **11**, 433 (2002).
[5] A. Zavriyev, E. Dupont, P. B. Corkum, H. C. Liu, and Z. Biglov, Opt. Lett. **20**, 1885 (1995).
[6] E. Dupont, P. Corkum, H. C. Liu, P. H. Wilson, M. Buchanan, and Z. R. Wasilewski, Appl. Phys. Lett. **65**, 1560 (1994).
[7] T. Maier, H. Schneider, M. Walther, P. Koidl, and H. C. Liu, Appl. Phys. Lett. **84**, 5162 (2004).
[8] M. H. Degani, M. Z. Maialle, P. F. Farinas, N. Studart, M. P. Pires, and P. L. de Souza, J. Appl. Phys. **109**, 064510 (2011).
[9] M. S. Kiledjian, J. N. Schulman, and K. L. Wang, Phys. Rev. B **44**, 5616 (1991).
[10] H. J. Lee, L. Y. Jurovel, J. C. Wolley, and A. J. Springthorpe, Phys. Rev. B **21**, 659 (1980).
[11] M. H. Degani and M. Z. Maialle, J. Comput. Theor. Nanosci. **7**, 454 (2010).
[12] D. Neuhasuer and M. Baer, J. Chem. Phys. **90**, 4351 (1989); 2180 (2005).
[13] Á. Vibók and G. G. Balint-Kurti, J. Phys. Chem. **96**, 8712 (1992).